TOXICOLOGICAL SCIENCES **127(1)**, 256–268 (2012)
doi:10.1093/toxsci/kfs067
Advance Access publication February 23, 2012

Distribution, Elimination, and Biopersistence to 90 Days of a Systemically Introduced 30 nm Ceria-Engineered Nanomaterial in Rats

Robert A. Yokel,*,†,[1] Tu C. Au,* Robert MacPhail,‡ Sarita S. Hardas,§ D. Allan Butterfield,§,¶ Rukhsana Sultana,§ Michael Goodman,§ Michael T. Tseng,|| Mo Dan,*,† Hamed Haghnazar,* Jason M. Unrine,||| Uschi M. Graham,|||| Peng Wu,[#] and Eric A. Grulke[#]

*Department of Pharmaceutical Sciences, College of Pharmacy, University of Kentucky Academic Medical Center, University of Kentucky, Lexington, Kentucky 40536-0596; †Graduate Center for Toxicology, University of Kentucky Academic Medical Center, University of Kentucky, Lexington, Kentucky 40506-0596; ‡Neurotoxicology Branch, U.S. Environmental Protection Agency, Research Triangle Park, North Carolina 27711; §Department of Chemistry, University of Kentucky, Lexington, Kentucky 40506-0055; ¶Center of Membrane Sciences, University of Kentucky, Lexington, Kentucky 40506-0059; ||Department of Anatomical Sciences & Neurobiology, University of Louisville, Louisville, Kentucky 40202; |||Department of Plant and Soil Sciences, University of Kentucky, Lexington, Kentucky 40546-0091; ||||Center for Applied Energy Research, University of Kentucky, Lexington, Kentucky 40511; and [#]Department of Chemical & Materials Engineering, University of Kentucky, Lexington, Kentucky 40506-0503

[1]To whom correspondence should be addressed at Department of Pharmaceutical Sciences, College of Pharmacy, University of Kentucky Academic Medical Center, University of Kentucky, Lexington, Kentucky 40536-0596. Fax: (859) 257-7564. E-mail: ryokel@email.uky.edu.

Received September 23, 2011; accepted January 16, 2012

Nanoceria is used as a catalyst in diesel fuel, as an abrasive in printed circuit manufacture, and is being pursued as an antioxidant therapeutic. Our objective is to extend previous findings showing that there were no reductions of cerium in organs of the mononuclear phagocyte (reticuloendothelial) system up to 30 days after a single nanoscale ceria administration. An ~5% aqueous dispersion of citrate-stabilized 30 nm ceria, synthesized and characterized in-house, or vehicle, was iv infused into rats terminated 1, 7, 30, or 90 days later. Cageside observations were obtained daily, body weight weekly. Daily urinary and fecal cerium outputs were quantified for 2 weeks. Nine organs were weighed and samples collected from 14 tissues/organs/systems, blood and cerebrospinal fluid for cerium determination. Histology and oxidative stress were assessed. Less than 1% of the nanoceria was excreted in the first 2 weeks, 98% in feces. Body weight gain was initially impaired. Spleen weight was significantly increased in some ceria-treated groups, associated with abnormalities. Ceria was primarily retained in the spleen, liver, and bone marrow. There was little decrease of ceria in any tissue over the 90 days. Granulomas were observed in the liver. Time-dependent oxidative stress changes were seen in the liver and spleen. Nanoscale ceria was persistently retained by organs of the mononuclear phagocyte system, associated with adverse changes. The results support concern about the long-term fate and adverse effects of inert nanoscale metal oxides that distribute throughout the body, are persistently retained, and produce adverse changes.

Key Words: **ceria; excretion; tissue distribution; rat; retention.**

Engineered nanomaterials (ENMs) have potential to contribute to applications that could produce intended (e.g., drug and gene delivery) or unintended (e.g., occupational and environmental) exposure. Understanding potential ENM toxicity lags behind application development, as is usually the case for new technologies. Insufficient understanding of ENM hazards could lead to human health problems and decreased public acceptance.

Ceria (cerium [Ce] oxide) ENMs have many current and potential commercial applications. Ceria is highly insoluble, including in phagolysosomal fluid at pH 4.5 (He *et al.*, 2010), and abrasive, enabling its use in chemical-mechanical planarization (integrated circuit manufacture) (Feng *et al.*, 2006). Most ceria applications capitalize on its redox activity, including as an oxygen sensor (Molin *et al.*, 2008), diesel fuel catalyst (increases combustion and converts carbon monoxide to carbon dioxide) (Cassee *et al.*, 2011; Health Effects Institute [HEI], 2001; Park *et al.*, 2007), in fuel cells (Yuan *et al.*, 2009), and for potential medical applications.

Therapeutic ceria ENM applications are generally based on its ability to reduce reactive oxygen species (ROS). Using many different cells in culture, ceria ENMs have been shown to reduce levels of H_2O_2, the superoxide radical, inducible nitric oxide synthase, nuclear factor-kappa B, tumor necrosis factor-α, interleukins, and other ROS endpoints. It has been suggested that ceria ENMs have utility in the prevention and/or treatment of cancer, diabetic cardiomyopathy, diesel exhaust– and cigarette smoke–induced oxidative stress, radiation therapy side effects, retinal degeneration, stroke, and neurodegenerative disorders (Babu *et al.*, 2010; Chen *et al.*, 2006; Colon *et al.*, 2010; D'Angelo *et al.*, 2009; Das *et al.*, 2007; Estevez *et al.*, 2011; Hirst *et al.*, 2009; Niu *et al.*, 2011; Xia *et al.*, 2008; Younce *et al.*, 2010). Ceria-mediated ROS reduction may relate to its properties as a superoxide dismutase mimetic and its catalase-like activity (Korsvik *et al.*, 2007; Pirmohamed *et al.*, 2010) and is perhaps attributed to Ce(III) rather than

Ce(IV) (Celardo *et al.*, 2011). Most of these studies were conducted in models of induced oxidative stress.

On the other hand, there are reports of ceria-induced toxicity, indicated by decreased cell viability, glutathione, and DNA content and increased lactate dehydrogenase release, malondialdehyde production, and apoptosis (Auffan *et al.*, 2009; Brunner *et al.*, 2006; Lin *et al.*, 2006; Park *et al.*, 2008). Most of these studies were conducted in non-ROS–stimulated cells. The reported effects of ceria ENM on nonmammalian organisms have generally been detrimental, including decreased growth, fertility, and survival and increased lipofuscin accumulation and susceptibility to oxidative stress, shown in *Pseudokirchneriella subcapitata* (green algae), *Synechocystis* PCC6803 and *Anabaena* CPB4337 (cyanobacteria), *Escherichia coli*, *Daphnia magna*, and *Caenorhabditis elegans* (Rodea-Palomares *et al.*, 2011; Roh *et al.*, 2010; Thill *et al.*, 2006; Van Hoecke *et al.*, 2009; Zeyons *et al.*, 2009; Zhang *et al.*, 2010). These studies do not inform about the long-term effects and fate of ceria ENM in the intact mammal, the target of medical applications and a receptor of unintended exposures.

Nanoscale ceria was identified for toxicity evaluation by the National Institute of Environmental Health Sciences (Integrated Laboratory Systems [ILS], 2006) and Organisation for Economic Co-operation and Development (OECD) Environment Directorate (OECD, 2010). The need for *in vivo* studies that examine its biokinetics and toxicity was recently identified (Cassee *et al.*, 2011).

A few studies with ceria ENM have been conducted in the intact mammal. Reduced myocardial oxidative stress was seen in transgenic mice that display ischemic cardiomyopathy (Niu *et al.*, 2007). Granulomatous inflammation was seen after pulmonary instillation and inhalation (Cho *et al.*, 2010; Srinivas *et al.*, 2011). Intravitreal injection reduced retinal vascular lesions (Zhou *et al.*, 2011).

Most therapeutic applications of ceria ENM will require systemic or pulmonary administration as its oral absorption is poor (~0.001%), although somewhat better from the lung (~0.1–1%) (He *et al.*, 2010; Hirst *et al.*, 2011; Yokel, Tseng, Dan, Unrine, Graham, Wu and Grulke, submitted for publication). Translocation can occur from the lung (and potentially other sites of uptake) to blood and ultimately all organs (He *et al.*, 2010). Therefore, the fate of ceria that is introduced into, or reaches, blood needs to be better understood.

Our previous research showed persistence in liver and spleen up to 30 days after systemic introduction of 5, 15, 30, and 55 nm ceria ENMs (Yokel, Tseng, Dan, Unrine, Graham, Wu and Grulke, submitted for publication). Ceria increased the protein oxidation marker protein carbonyl (PC) levels in liver 30 days after 5 nm ceria ENM treatment. Ceria-containing macrophages were seen in the spleen and liver 30 days after 5 and 30 nm ceria ENMs, associated with hepatic granulomas comprised of Kupffer cell cores, surrounding mononucleated cells, and CD3 positive T lymphocytes (Tseng *et al.*, 2012).

The present study was conducted to test the hypotheses that a significant amount of ceria ENM persists in the mammal beyond 30 days and that adverse tissue changes seen 30 days after ceria administration progress. The objectives were to ascertain the distribution, translocation, elimination, and selected biological effects (including histopathology and oxidative stress) for 90 days after a single iv ceria ENM infusion. The iv route was selected to model the ceria that would enter systemic circulation after translocation from any uptake site, such as the lung, as well as its iv administration, as might be employed when used as a therapeutic agent.

MATERIALS AND METHODS

Nanomaterial. A ~5% aqueous citrate–stabilized ceria dispersion was synthesized using a hydrothermal approach (Mai *et al.*, 2005). It was citrate coated (capped) to prevent the agglomeration seen with uncoated ceria that occurs in high-ionic strength solutions, such as blood (Xia *et al.*, 2008). Citrate is a commonly used surface coating agent for ENMs, a component of blood (~100μM in humans), and has been shown to have no effect on erythrocyte response to a silver ENM (Choi *et al.*, 2011). Generally, a 20 ml aqueous mixture of 1 mmol cerium nitrate and 105 mmol sodium hydroxide was stirred for 0.5 h. This produced a milky suspension that was transferred into a Teflon-lined stainless steel bomb and heated at 180°C for 24 h. The fresh white precipitate was then washed with deionized water three times followed by ethanol three times to remove free cerium and organic impurities. The wet precipitate was then dispersed into 0.05M citric acid aqueous solution with stirring overnight, followed by washing with water five times. The resulting dispersion had a pH of 3.9. It was sterilized by autoclaving. To determine whether autoclaving affected the ceria ENM concentration, quadruplicate samples of the dosing material were prepared for Ce analysis before and after autoclaving. Eleven samples of the dosing material were digested by two methods and analyzed by inductively coupled plasma mass spectrometry (ICP-MS) to quantify ceria content (Yokel *et al.*, 2009). It was 5.2 ± 0.1%. Based on the volumes infused, the dose given the rats was ~87 mg ceria/kg. The autoclaved ceria ENM was iv infused without any further treatment.

Ceria characterization. The morphology, crystallinity, and particle size distribution of highly diluted samples of the citrate-coated ceria ENM were determined in our laboratories using high-resolution transmission electron microscopy (TEM)/scanning TEM and X-ray diffraction analyses/scanning TEM (200-keV field emission analytical transmission electron microscope [JEOL JEM-2010F; Tokyo, Japan] equipped with an Oxford energy dispersive X-ray spectrometer). The primary particle size was determined using Gatan software (DigitalMicrograph 3.7.1; Pleasanton, CA) by sizing 110 particles. From the data of individual primary particle sizes measured from the TEM images, a number frequency cumulative distribution was constructed. The cumulative distribution was best described by a log-normal distribution model, characterized by a sample mean and a SD. The data were well described by a monomodal distribution, e.g., one continuous distribution was observed with no significant secondary or tertiary peaks. The reported "average" diameter of each sample was $D_{ave} = \exp(\mu) D_{ave} = \exp(\mu)$, where μ is the mean of the log-normal probability distribution, and the reported "SD" is the value from the fit of the log-normal distribution to the data. A number-based differential frequency distribution was constructed using the model coefficients. The ceria nanoparticles were crystalline and highly pure as determined by X-ray diffraction (Siemens 5000 diffractometer). Particle size distribution in aqueous dispersion was determined using dynamic light scattering (90Plus Nanoparticle Size Distribution Analyzer; Brookhaven Instruments Corp., Holtsville, NY). The surface area of the dried powder was determined by isothermal nitrogen adsorption using a BET surface area analyzer (Tristar 3000; Micromeritics Instrument Corporation, Norcross, GA). To indicate the stability of the ceria dispersion when infused into the rat, the zeta potential was measured using

a Zetasizer nano ZS (Malvern Instruments, Worcestershire, U.K.). Because the ceria ENM had a hydrodynamic diameter < 200 nm, the Hückel approximation was used to calculate zeta potential from electrophoretic mobility. Scanning transmission electron microscope (STEM) images were acquired using the high-resolution probe at 2 Angstrom in a 2010F STEM outfitted with a ultrahigh resolution pole piece, GATAN 2000 GIF, GATAN DigiScan II, and EmiSpec EsVison software. The ceria ENM was analyzed prior to administration using electron energy loss spectroscopy (EELS) to determine its M_4/M_5 ratio as a measure of its original oxidative signature. EELS measurements were performed using the 2 Angstrom probe, an alpha of 20 mrad, and a beta of 6 mrad to estimate the Ce(III) versus Ce(IV) oxidation states using the cerium M_4 and M_5 edges and M_4/M_5 ratio. The interior of the 30 nm ceria ENM and the exterior particle surface were separately analyzed. To estimate the extent of citrate surface coating, the ceria ENM was washed at least three times with water before drying. Thermogravimetric analysis (Perkin-Elmer TGA7 Analyzer) was then performed to determine the weight loss of the citrate-coated ceria ENM from 150°C to 300°C over which decomposition of citric acid occurs. The extent of citrate surface coating was estimated based on the assumption that the ceria ENM was spherical and had a uniform size. The free Ce concentration in the washed ceria ENM dispersion was determined using Amicon Ultra-4 centrifugal 3000 molecular weight cutoff filter devices and centrifugation at 3000 × g to obtain filtrate, which was analyzed by ICP-MS.

Animals. The results of this study are from 31 male Sprague Dawley rats, weighing 300 ± 19 g (mean ± SD), purchased from Harlan. They were housed individually prior to study and after cannulae removal (a few days after the iv infusion) in the University of Kentucky, Division of Laboratory Animal Resources facility under a 12:12 h light:dark cycle at 70 ± 8°C and 30–70% humidity. The rats had *ad libitum* access to 2018 Harlan diet and reverse osmosis water. Animal work was approved by the University of Kentucky Institutional Animal Care and Use Committee. The research was conducted in accordance with the Guiding Principles in the Use of Animals in Toxicology.

Ceria administration. In initial studies, unanesthetized rats were infused iv with ~100 mg ceria ENM dispersion/kg using described procedures (Yokel *et al.*, 2009). Rats tolerated the ceria infusion well. Therefore, the test doses were ~100 mg ceria/kg (found by analysis to be 87 mg ceria/kg, equivalent to 70 mg Ce/kg) infused over 1 h or water (controls for ceria vehicle) adjusted to pH 3.9 infused over 1 h. This large ceria ENM exposure was utilized to enhance our ability to detect Ce in multiple tissues and fluids up to 90 days after the single infusion. Fifteen rats were infused with vehicle and 16 with ceria. Three control and three ceria-treated rats were terminated 1, 7, or 30 days after completion of the infusion. Six control and seven ceria-treated rats were terminated 90 days after the infusion. All rats were cageside observed daily to assess respiratory, musculo-nervous, ophthalmic, and other abnormalities (the presence of dyspnea, tachypnea, tremor, ataxia, head tilt, hyperactivity, hypoactivity, lethargy, paralysis, opacity of the eyes, dilated/constricted pupils, exophthalmia, enophthalmia, conjunctivitis, abnormal secretions/crusting of the eyes, corneal ulcers, diarrhea, ruffled fur, urine staining, and other notable observations). Each was weighed weekly. Rats scheduled for termination at 7, 30, or 90 days were housed in metabolic cages from 3 days before until the 7th or 14th day after infusion. Urine and feces were collected daily from six control and eight ceria ENM–treated rats to 7 days and six control and five ceria ENM–treated rats to 14 days.

Ceria distribution and elimination. Daily urine volume was determined. Daily feces weight was determined as the wet feces and after drying to constant weight. At termination, the brain, lung, thymus, heart, spleen, liver, adrenal, right kidney, and right testis were rapidly removed and weighed. Samples were obtained for Ce analysis from brain cortex, lung, thymus, heart (horizontal medial cross-section), spleen (medial tip), liver (near tip of the larger of the two bifurcated lobes), adrenal, right kidney (medial cross-section), intestine (a 1 cm segment 5–6 cm below the pyloric sphincter), testis (internal issue), skeletal muscle from the right femur, skin (from the middle of the back), bone marrow (tibia), whole blood (vena cava), and cerebrospinal fluid (CSF) (withdrawn from the cisternomedullary space). The skeletal system was cleaned by Dermestidea beetles, cleaned of beetle residue by placing the skeleton in deionized water in a Ziploc bag, which was sonicated in a bath sonicator for 15 min, washed with deionized water, dried, and weighed.

Samples of each collected tissue and fluid, and skeletal system samples from the cranium, spinal column, ileac crest (pelvis), and femur (representative of the appendages), and the rat chow consumed by these subjects were prepared and analyzed for Ce by ICP-MS (Agilent 7500cx; Santa Clara, CA) as previously described, which reported the method detection limit (MDL) of Ce in tissue of 0.089 mg Ce/kg and 0.018 mg Ce/l in blood or serum samples (Yokel *et al.*, 2009). The procedures to prepare and analyze the samples are described in the Supplementary information. Cerium concentrations below the MDL were reported as 50% of the MDL. Organ/system Ce concentration in all tissues/fluids as well as mass amount of Ce and percent of the ceria dose in the rat were calculated, the latter from the organ weight or based on 0.02, 1.8, 50, 20, 3, and 7% of the body weight for the adrenal gland, intestine, skeletal muscle, skin, bone marrow, and blood, respectively. The skeletal system was separated into four components (cranium, spinal column, pelvis, and femur), which constituted 21, 38, 10, and 31% of its weight, respectively.

Tissue preparation and histological evaluation. After termination of ketamine-anesthetized rats, harvested tissue samples were immediately immersed in 10% neutral buffered formalin and subsequently processed by paraffin embedding for histopathology analysis. Sections (5 μm) were cut and stained with hematoxylin and eosin and examined for qualitative and quantitative changes. For plastic embedding, tissues were cut into 3 mm^3 pieces, postfixed in osmium tetraoxide, dehydrated, and embedded in Araldite 502. One-micron sections were cut and stained with toluidine blue. All sections were coded and examined by an experienced histologist and an experimental pathologist.

Oxidative stress assessment. PC levels, as a global marker for protein oxidation and oxidative stress, were measured in liver and spleen using a specific antibody and slot blot technique as described (Butterfield, 1997; Sultana *et al.*, 2005). The liver and spleen were examined because they had the highest ceria concentrations.

Data and statistical analysis. Grubb's test was used to identify outliers in fluid, tissue, urine, and feces Ce results. A two-way ANOVA was used to compare body weights of rats terminated 90 days after treatment, normalized to their treatment day weight. Organ weights, not and normalized to body weight, were compared by one-way ANOVAs followed by Tukey's multiple comparison tests and unpaired *t*-tests. The percentage of the ceria dose in the liver, spleen, kidney, heart, lung, brain, thymus, and testis was calculated based on each rat's whole organ weight times its Ce concentration, correcting for Ce as a percentage of ceria. Median pretreatment 24 h-urine and feces Ce excretion obtained from 24 rats was subtracted from posttreatment values of ceria-treated rats to obtain the excretion of Ce attributable to treatments. The concentration of Ce and percent of dose in all sampled tissues and fluids and of the four skeletal system regions were compared by two-way ANOVAs and Bonferroni multiple comparisons. One-way ANOVAs with Tukey tests were also conducted to determine differences in the percent of dose across time in each sampled tissue or fluid and across tissues and fluids at the same time. Results are reported as mean ± SD, except for the PC levels in ceria-treated rats, which were normalized to their respective control samples and expressed as % mean ± SEM. Significance was accepted at $p < 0.05$.

RESULTS

Nanomaterial

High-resolution (HR)-TEM/HR-STEM showed the ceria ENM was crystalline (its only known structure is face-centered cubic) (Fig. 1A). It had Miller indices of (111), (220), and (311), and with lesser presence of (200), (222), and (400), based on X-ray diffraction crystal structure linked to known morphology. Its average (and SD) primary particle diameter was 31.2 (17.1) nm. The particle size distribution was bimodal.

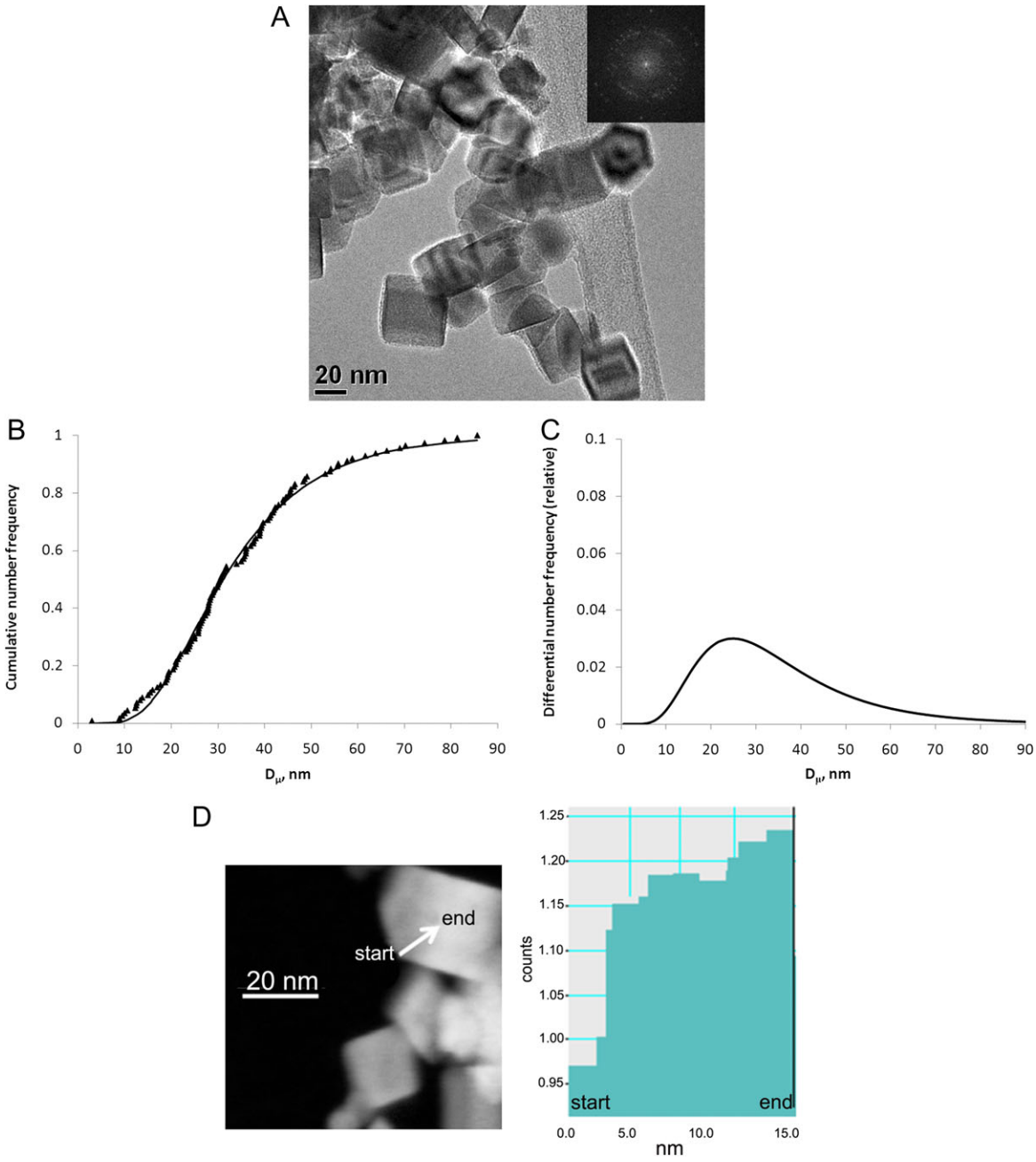

FIG. 1. Panel A: TEM image of 30 nm ceria showing cubic particles. The insert in the top right hand corner is an electron diffraction pattern verifying the ceria crystallinity. Panels B and C: Primary particle size distribution of the ceria ENM, as determined by TEM, showing cumulative and differential frequency distributions. Panel B shows the TEM size distribution data as points and a lognormal model as a continuous curve. Panel C shows the differential distribution as represented by the lognormal model. Panel D: HR-STEM image of the as-produced ceria ENM. EELS analyses were conducted along the indicated trace line (arrow) starting at the exterior rim or surface layer and ending in the core region. The computed M_4/M_5 ratio shows the change in the oxidation state.

The peaks were centered at 41 and 273 nm; the percentages of each peak were 100:0 (number basis) and 36:64 (volume basis). Figure 1B shows the fit of the lognormal model (continuous curve) to the cumulative distribution (number frequency basis). Figure 1C shows the differential distribution computed from the model coefficients. Note that, for a log-normal distribution, the mean of the distribution, μ, is not the peak of the differential distribution but is displaced to a slightly higher diameter. Primary ENM particles can agglomerate (self-associate) in aqueous dispersions, yielding particles that tend to associate with each other rather than the TEM grid (Fig. 1A). Different weighting factors that can be used to estimate average ENM size, including number based (typically the result of TEM diameter measurements), volume based (which is dose

related as it links directly to the mass of ENM of a specific size), and intensity (the signal from the light scattering experiment). The bimodal distribution demonstrates that agglomeration occurred for this ENM. The BET-determined surface area was 15 m^2/gm, which would correspond to an average diameter of 52 nm. The estimated differences between the TEM and BET methods suggest that this ENM may self-associate with one whole face to form agglomerates, reducing its apparent surface area. Some face-to-face agglomerates can be seen in Figure 1A. The zeta potential in water at pH ~7.3 was −56 (± 8) mV. The EELS results show that the surface of the ENM had a slightly reduced valency at its outer rim and a more enhanced valency (less reduction) in the central (core) region. This was observed as a change in the height of the sharp intense peaks at the cerium M_5 and M_4 edges (~883 and 900 eV). A representative EELS line scan from the exterior surface toward the inner zone of the ceria shows the enrichment of Ce(III) at the particle rim (surface layer) (Fig. 1D). The extent of surface citrate coating was ~18%. The free Ce content was << 1%. Cerium concentration after autoclaving was 99.1% of that seen prior to autoclaving.

Animal Observations

All ceria-treated rats survived for their assigned study duration. Daily cage-side observations revealed no adverse effects. There was no significant difference in daily wet feces outputs during the first week between ceria-treated and control rats. The only significant differences in urine outputs were greater output on day 3 among the ceria-treated rats terminated at 1 week compared with many of the other groups and a lower output on day 4 compared with some groups. Ceria ENM–treated rats showed a reduced body weight gain shortly after ceria administration (Fig. 2). ANOVA results showed significant effects of treatment and time but not a significant interaction. The spleen of many ceria-treated rats showed punctate white specs. The only organ showing a significant difference in weight between control and treated rats was the spleen. This was not revealed by the one-way ANOVA ($p = 0.108$); however, two-tailed unpaired *t*-tests showed the treated rats to have significantly heavier spleens at 1 and 30 days (non and normalized to body weight) and significantly lighter at 7 days (not normalized to body weight) (Fig. 3).

Ceria Distribution and Elimination

Grubb's test revealed six outlier Ce concentration results, among 304 tissue/fluid × termination time × treatment conditions for the ceria ENM–treated rats. Among the 283 tissue/fluid samples from the control rats, 231 were below the MDL, versus 19 of the 304 from treated rats, which were mainly brain (all three at 1 week and 1 month and three at 3 months) and CSF (two at 1 day and two at 1 week).

Baseline (preceria ENM treatment) 24 h urinary and fecal Ce excretion medians were 0.038 and 1.04 μg, respectively. One post-Ce treatment feces value was an outlier. When pre-treatment 24 h median Ce excretion was subtracted from total Ce excretion postceria ENM dosing, ~2 and 100 μg of ceria appeared in the urine and feces in the first 2 weeks, representing ~0.01 and 0.5% of the dose, respectively (Fig. 4).

Tissue/fluid Ce concentration results are shown in Figure 5A and expressed as a percentage of the ceria dose in Figure 5B. Brain cerium concentration, corrected for the cerium in the blood vessels of the brain, in concert with extensive light and electron microscopic observations, suggested very little ceria ENM crossed the blood-brain barrier into brain cells. A two-way ANOVA of Ce concentration across time and among sampled tissues and fluids $F(3,14,42) = 2.9$, 25.9, and 2.24 showed significant effects of time, site, and interaction ($p = 0.036$, $p < 0.0001$, and $p = 0.0001$, respectively). Bonferroni comparisons only showed a significant decrease of Ce in spleen from day 1 compared with days 7 and 30 followed by a significant increase from days 7 and 30 compared with day 90. A two-way ANOVA of the percent of the dose across time and among sampled tissues and fluids $F(3,14,42) = 4.06$, 56.2, and 2.48 showed significant effects of time, site, and interaction ($p = 0.008$, $p < 0.0001$, and $p < 0.0001$, respectively). Bonferroni comparisons only showed reductions

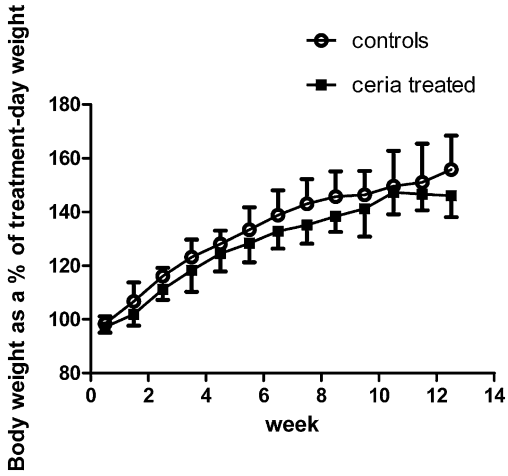

FIG. 2. Body weight of control and ENM ceria–treated rats after treatment.

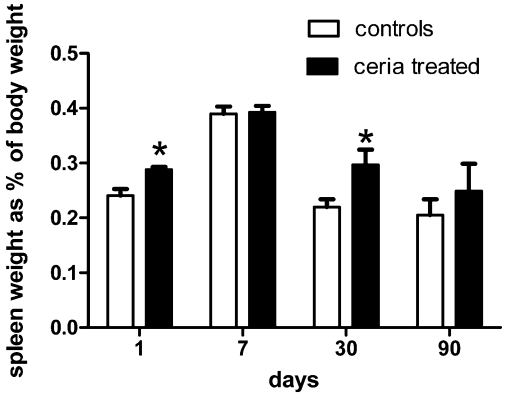

FIG. 3. Spleen weight, as a percent of body weight. *Significantly different from control at same time by *t*-test.

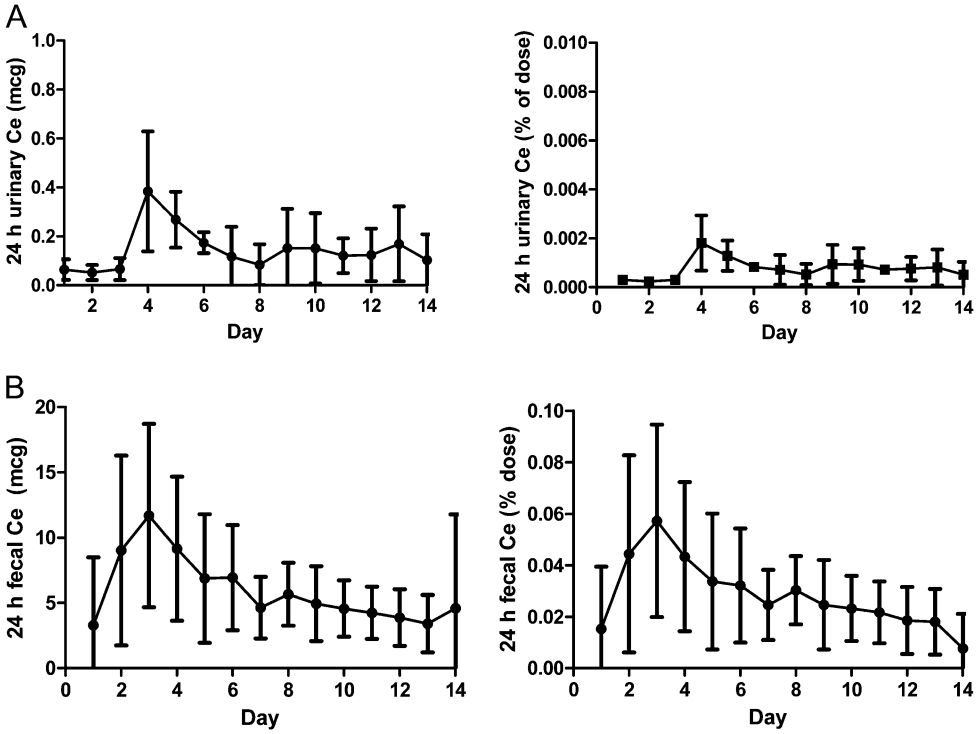

FIG. 4. Daily urine (A) and fecal (B) Ce excretion of five ceria-treated rats, as mass amount (left panels) and as a percentage of the dose (right panels). Note the 50-fold difference in the y-axis scales between urine and feces.

in the percent of the dose in liver and bone marrow over time and an increase in the spleen but no differences among the sampled sites. The lack of other significant differences might be due to the large number of comparisons in this analysis. Therefore, one-way ANOVAs with Tukey tests of the percent of the dose in each sampled site over time were conduced. They revealed significant reductions in the heart (from day 1 to days 7, 30, and 90) and the brain (from day 1 to day 90). When all sample sites were compared at a single time (1, 7, 30, or 90 days), liver was higher than all sites but bone marrow, and bone marrow was higher than all other sites at day 1; liver and bone marrow were higher than all other sites at day 7; liver was higher than all sites except bone marrow at day 30; and liver was higher than all sites but spleen, spleen was higher than all sites but bone marrow, and bone marrow was higher than all other sites but blood at day 90. These results show little decrease of Ce in the sampled sites over time; much more ceria in the liver, bone marrow, and spleen than other sites; and evidence of translocation to the spleen at day 90. Figure 6 shows the ceria in the four skeletal system regions studied. Two-way ANOVAs showed significant effects of time and region for Ce concentration and percent of dose but not interaction $F(3,3,9) = 3.82$, 5.82, and 0.98 ($p = 0.0157$, 0.0018, and 0.47, respectively). The significant differences are shown in Figure 6. The spinal column and pelvis had considerably higher Ce concentration than the femur and cranium.

The mean rat chow Ce concentration was 0.22 mg Ce/kg. Given that Sprague Dawley rats eat ~5 g food/100 g body weight daily (http://www.aceanimals.com/SpragueDawley.htms), the daily Ce intake from food of these rats would be ~4.4 μg, and over 90 days 0.3 mg, or less than 2% of the Ce in the 87 mg ceria/kg iv dose. Cerium is poorly absorbed from the gastrointestinal tract (Durbin *et al.*, 1956; Gehlhaus *et al.*, 2009; Miller and Byrne, 1970), as is ceria ENM (He *et al.*, 2010; Hirst *et al.*, 2011; Park *et al.*, 2009). Therefore, Ce in the rat chow did not significantly contribute to blood and tissue Ce levels.

Liver, spleen, and bone marrow showed the most avid uptake and retention of ceria ENM. The ceria-containing Kupffer cells situated in the sinusoids became visible by light microscopy 1 day after infusion. Less visible was hepatocellular accumulation. The continued presence of ceria after the single vascular infusion was associated with hepatic granuloma formation first seen after 30 days that persisted in the 90-day samples in all ceria-infused rats. These intrasinusoidal cellular agglomerates comprised a core of Kupffer cells surrounded by mononucleated cells. In spite of the granulomatous formation, hepatic parenchyma remained viable (Fig. 7A). Occasional perivascular accumulation of lymphocytes was also observed, and one T-cell population in the granuloma was identified by CD3 immunohistochemistry (Wang *et al.*, 2009). In the enlarged spleen, histological examination showed ceria-containing macrophages both in the red and white pulp in 30- and 90-day samples (Fig. 7B). In the brain, unlike systemic tissue rich in mononuclear phagocyte cells, light microscopy did not reveal cells with ceria accumulation in neurites or the microvessels in the hippocampus (Fig. 7C) or the cerebellum (Fig. 7D).

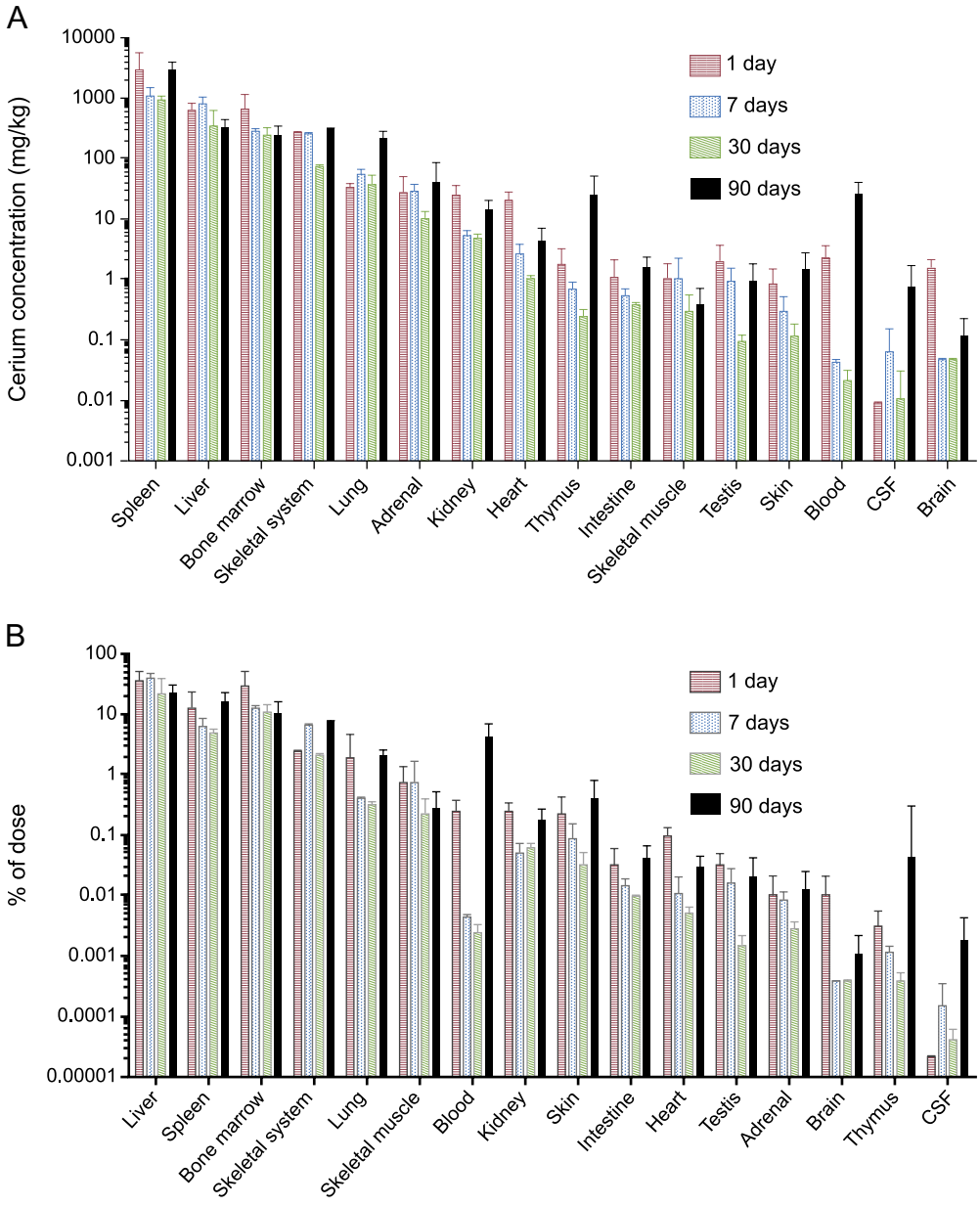

FIG. 5. Cerium concentration (A) and percent of the dose (B) in tissues, blood, and CSF. Skeletal system Ce concentration is the mean of the four regions, and % of dose is the sum.

Oxidative Stress Assessment

PC levels were increased significantly in liver after 1, 7, and up to 30 days and later decreased significantly 90 days after ceria treatment (Fig. 8A). On the other hand, PC levels were decreased significantly 1, 7, and 90 days after ceria treatment in spleen (Fig. 8B).

DISCUSSION

The present study utilized an established 90-day toxicity protocol (1, 7, 30, and 90 days) to study the short- and long-term effects of a single dose of a nanoscale ENM, as was employed to study the effects of intratracheal nanoscale quartz instillation (Warheit *et al.*, 2008). The study used an in-house synthesized 30 nm cubic ceria that was well characterized, as required by this journal and advised by many (Bouwmeester *et al.*, 2011; Maynard *et al.*, 2011; Powers *et al.*, 2009; Sayes and Warheit, 2009).

The present study extends prior work that showed persistence of nanoscale ceria in mice and rats for up to 7 and 14 days after its oral administration, 7 days after the last ip injection, 28 days after its intratracheal instillation, and 30 days after its systemic introduction (He *et al.*, 2010; Hirst *et al.*,

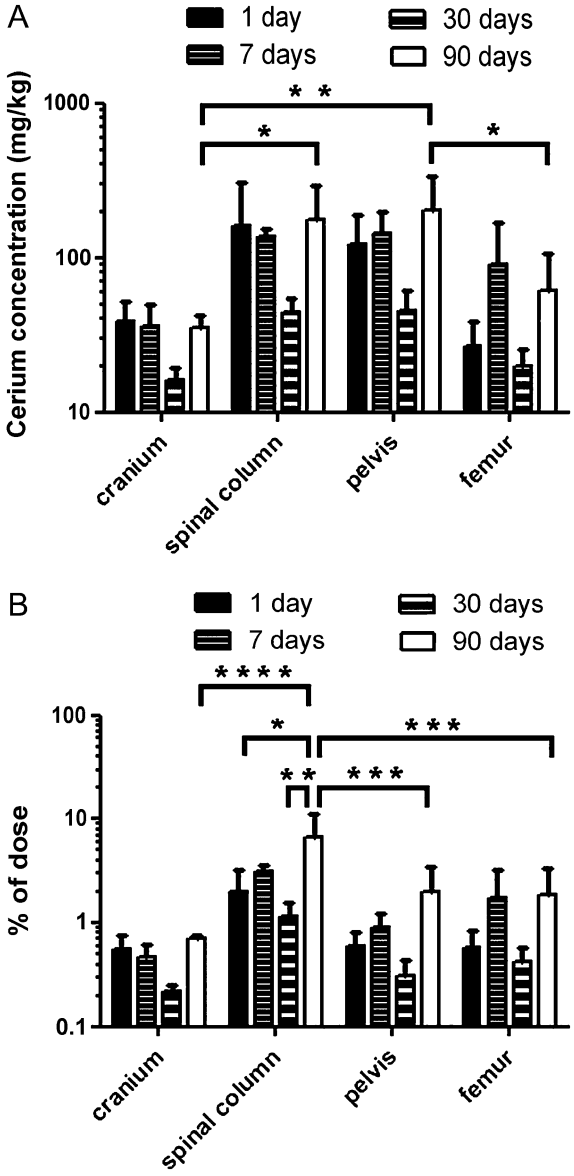

FIG. 6. Cerium concentration (A) and percent of the dose (B) in the four skeletal system regions. Significantly different *$p < 0.05$, **$p < 0.01$, ***$p < 0.001$, and ****$p < 0.0001$.

2011; Park *et al.*, 2009, 2010; Yokel, Tseng, Dan, Unrine, Graham, Wu and Grulke, submitted for publication). The present study extended the determination of ceria in the rat up to 90 days and determined ceria in several more tissues and fluids than previously reported (bone marrow, which is a major site of ceria ENM distribution and adrenal, thymus, skin, and CSF), providing a more complete assessment of its fate. The use of a large ceria ENM dose enabled us to see cerium in all sampled tissues and fluids up to 90 days, in comparison to prior work, some of which employed lower doses. Additionally, this study employed both ICP-MS and electron microscopy to determine ceria distribution, providing insight into the subcellular localization of the ceria. By determining multiple endpoints in one study, namely ceria disposition and persistence, subcellular localization in selected tissues, safety as cage-side observations, effects assessment including PCs as a major indicator of oxidative stress and histological evaluation, and determination of the valence of nanoceria *in vivo* which has not been previously reported by anyone, this study enabled the interpretation of the temporal interrelationship of these endpoints.

The short-term reduction of body weight gain compared with controls has been previously observed after high dose intratracheal instillation of ceria ENM (~130 nm ceria given to mice Park *et al.*, 2010). Given the large dose of ceria ENM, body weight gain reduction is not unexpected. The lack of morbidity (observable clinical toxicity) and mortality over the 90 days shows this dose of the studied ceria ENM did not produce profound toxicity, although abnormal changes were observed in the liver and spleen, discussed below. Splenomegaly after ENM exposure was reported after iv administration of a 49 nm magnetite-dextran ENM (Okon *et al.*, 2000) and seen 30 days after a single iv administration of 5, 15, and the same 30 nm ceria ENM (Yokel, Tseng, Dan, Unrine, Graham, Wu and Grulke, submitted for publication). The cause of this finding will require further study.

The very small clearance of ceria, nearly all into feces, during the first 2 weeks after ceria ENM administration has been previously noted, although the prior studies did not quantify urinary cerium excretion after oral, intratracheal, iv, or ip ceria ENM administration (He *et al.*, 2010; Hirst *et al.*, 2011). Given that the ceria ENM was not eliminated to any significant extent, its prolonged retention is not surprising. Ceria, as Ce, was detectible in all tissues and fluids sampled at 90 days. There was no appreciable clearance of the ceria ENM over the 90 days, which was mostly present as intracellular ceria agglomerations in mononuclear phagocyte system tissues. Of the 64% of the ceria ENM dose found in the sampled organs and fluid compartments 90 days after its administration, 72% was in the liver, spleen, and bone marrow. This is consistent with the accumulation of other insoluble metal and metal oxide ENMs in the liver, spleen, and bone marrow (e.g., Ballou *et al.*, 2004; Choi *et al.*, 2007; Fabian *et al.*, 2008; Moghimi *et al.*, 2001). Given the lack of ceria ENM clearance, it is assumed that a single large ceria ENM dose would model tissue cerium levels after repeated, smaller, doses. We have found that the percentage of the dose of a 5 nm ceria ENM in the liver is comparable after a single iv administration of 11 mg ceria/kg, five administrations of this dose given over consecutive days, and a single administration of 56 mg ceria/kg (Yokel, Michelli, Haghnazar, Unrine, Wu, Grulke, unpublished results).

Prior studies found granulomas in the lung 7 days and in lymphocytes 14 days after ~130 nm ceria given intratracheally to mice (Park *et al.*, 2010). Multifocal microgranulomatous changes were seen in the lung by day 14 of daily head-and-nose-only inhalation of 15–30 nm ceria ENM, and granulomatous changes were observed in the lung 28 days after ceria ENM instillation into lungs of rats (Cho *et al.*, 2010; Srinivas *et al.*, 2011). Other than the observation of granulomas

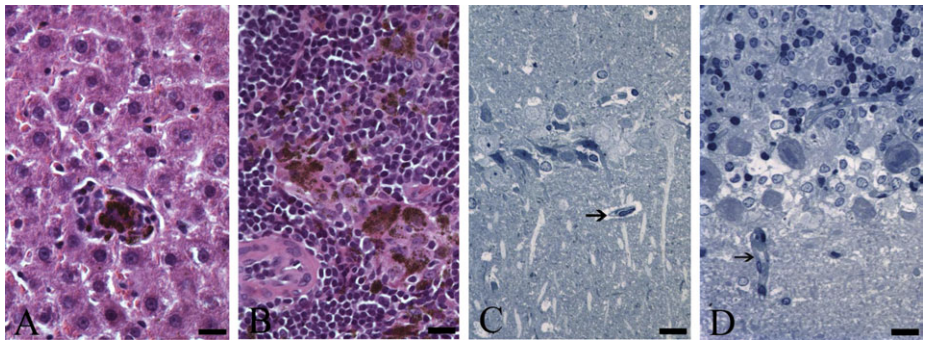

FIG. 7. Histology of liver, spleen, hippocampus, and cerebellum 90 days after ceria ENM infusion. Panel A shows the normal appearing liver with a granuloma formation. Panel B was taken from the white pulp of a spleen showing phagocytic cells with ceria particulates. Panel C illustrates a CA1 pyramidal cell and adjacent small vessel (arrow), both free of ceria. Panel D shows cerebellar tissue and the absence of ceria in both the neuronal and vascular components (arrow).

in a few rats that received the lowest of the three doses of silver ENM by inhalation (Sung *et al*., 2009), the current study seems to be the first report of granulomatous changes in the mammalian liver after metal or metal oxide ENM administration. No progression or diminution of the granulomatous changes in the liver was seen over the 90 days. The long-term fate and effect of this inflammatory reaction are unknown.

One of the mechanisms by which nanomaterials interact with biological systems is by generation of free radicals (Nel *et al*., 2006). Depending on the reactivity and half-life of free radicals, they can interact with and damage proteins, lipids, and nucleic acids. Apart from other important cellular functions, proteins can function as antioxidant enzymes or molecules, which comprise the cellular defense against free radical–mediated oxidative stress. The interaction between proteins and free radicals may change the 3D structure of proteins by oxidative modification of the protein backbone or amino acid residues (Stadtman, 2006). A change in its 3D structure may affect or inhibit protein functions. The extent of oxidative damage of a protein can be estimated by PC levels, a global marker for protein oxidation. Therefore, PC levels were measured in control and ceria-treated rat liver and spleen samples. Increased PC levels in liver were found at most time points examined. These results confirmed earlier findings on liver PC at 30 days following a single iv 5 nm ceria ENM infusion (Tseng *et al*., 2012). There are few *in vitro* and *in vivo* studies reporting hepatotoxicity of nanomaterials which also reported pro-oxidant effects of ENM treatment (Hussain *et al*., 2005; Loh *et al*., 2010; Patlolla *et al*., 2011; Sayes *et al*., 2005; Yuan *et al*., 2011). Although many studies reported ENM accumulation in the spleen (Ballou *et al*., 2004; Choi *et al*., 2007; Fabian *et al*., 2008; Moghimi *et al*., 2001), oxidative stress effects of ENM treatment were not investigated. A recent study reported no effect on inflammatory cytokine release from spleen macrophages after magnetic Fe_2O_3 ENM treatment (Wang *et al*., 2011). In contrast to liver, PC levels were decreased in the spleen at each time point examined (but statistical significance for the results at 30 days was not reached). This difference in response from liver and spleen cells to ceria ENM treatment may be due to differences in the cellular types in these organs. Interestingly, after 90 days, ceria ENM induced antioxidant effects in both organs. Consequently, our findings suggest that there is a time dependence to the effects of ceria treatment with respect to peripheral organs. These effects may relate to the oxidation state of the ceria ENM (Celardo *et al*., 2011; Korsvik *et al*., 2007; Pirmohamed *et al*.,

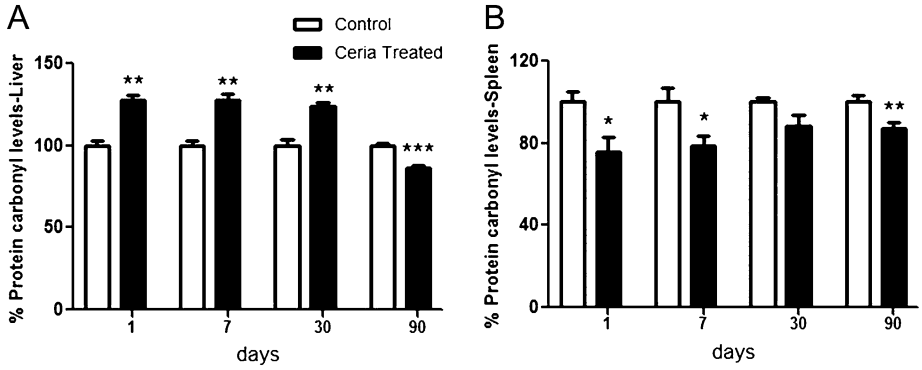

FIG. 8. Panel A histogram represents PC levels in liver 1, 7, 30, and 90 days after ceria treatment measured in control and ceria-treated rats. Significant difference reported for $^{**}p < 0.01$ and $^{***}p < 0.001$. Panel B histogram represents PC levels in spleen, 1 day, 7 days, 30 days, and 90 days after ceria treatment measured in control and ceria-treated rats. Significant difference reported for $^{*}p < 0.05$ and $^{**}p < 0.01$.

2010), which we found to be enriched with Ce(III) at the particle surface in this study. As there is a very limited literature available on short-term and long-term effects of ENM treatments, it is difficult to discuss the variation in the oxidative stress response within an organ or from organ to organ. Therefore, short- and long-term effects of ENM treatment on redox status of liver and spleen are under further investigation.

Ceria is considered an inert material, from a solubility standpoint. However, due to its redox catalytic properties, it has significant chemical activities, for which it is used and being pursued in many applications, as noted in the Introduction section. Its lack of solubility probably contributes to its persistence, and its catalytic activity probably contributes to its effects on oxidative stress endpoints. It is unclear if the adverse effects seen in the liver and spleen are due to mechanical irritation from its presence or its chemical (catalytic) activity. These results further support the concern about inert nanoscale metal oxides that are introduced into, or reach, systemic circulation, from which they can distribute throughout the body and result in persistent retention and potential adverse effects in multiple organs.

The present results provide information assessing the health effects of nanoceria. Although much was learned about the distribution and retention of ceria ENM and concurrent effects, there are limitations to this, and any, study. One is the use of a laboratory-generated ENM for study, which might not be representative of commercial nanoceria. Indeed, our initial study utilized a commercial ceria ENM; however, we were unable to obtain from the supplier some characterization information needed to fully understand the ENM (Yokel *et al.*, 2009). This led to our decision to manufacture and characterize in-house our ENM study materials, enabling us to better understand the material we are studying. As noted in the Introduction section, nanoceria is utilized in multiple applications. These would represent different physicochemical forms, with different surface capping agents and in different dispersing media, or as solids. It is not feasible, timewise or economically, to characterize well all nanomaterials (Choi *et al.*, 2009), making it necessary to extrapolate or use other approaches such as tiered testing systems and grouping (banding) similar ENMs. For this study, we selected a ceria ENM size that appears to be in the range where ENMs are most different from the effects of their solution or bulk scale components, based on protein binding (Nel *et al.*, 2009), cell uptake (Chithrani *et al.*, 2006), and induction of acellular oxidative stress (Jiang *et al.*, 2008). It is anticipated that ceria ENM solubility would not be influenced by size, which relates to persistence, a major focus of this study. We must also realize that ENMs are highly reactive and therefore their composition can change in the body of the organism exposed to them, e.g., by opsonization, and in the environment. It is important to begin investigations on the kinetics and effects of nanomaterials of known composition. The present results add to prior knowledge about ceria ENMs and identify some of the issues that warrant further study to more fully characterize their health effects.

CONCLUSIONS

A single ceria ENM administration initially reduced body weight gain. Cerium excretion following ceria ENM infusion was 98% in the feces and very slow, resulting in elimination of < 1% of the dose in the first 2 weeks. Spleen weight was greater at most times after ceria ENM administration, associated with visual and microscopic evidence of abnormality. Nanoscale ceria was retained in mononuclear phagocyte system tissues from which there was little clearance over 90 days, supporting the hypothesis that a significant amount of ceria ENM persists in the mammal well beyond 30 days. However, the lack of morbidity, mortality, or significant progression (or regression) of adverse changes in the liver and spleen fails to support the hypothesis of progression of untoward effects beyond 30 days. The long-term effects of nanoscale ceria that enters cells warrant investigation, considering the near irreversibility of its accumulation.

SUPPLEMENTARY DATA

Supplementary data are available online at http://toxsci.oxfordjournals.org/.

FUNDING

This work was supported by United States Environmental Protection Agency Science to Achieve Results (grant number RD-833772). Although the research described in this article has been funded wholly or in part by the United States Environmental Protection Agency through STAR Grant RD-833772, it has not been subjected to the Agency's required peer and policy review and therefore does not necessarily reflect the views of the Agency and no official endorsement should be inferred. Support was provided to T.C.A. (Summer Undergraduate Research Program) from The Pharmaceutical Sciences Department and Office of the Dean, College of Pharmacy, University of Kentucky.

ACKNOWLEDGMENTS

The authors gratefully acknowledge Dr Jim Krupa, University of Kentucky Biology Department, for his Dermestidea beetle colony that cleaned the skeletons and Rebecca L. Florence and Caleb Morris for their excellent contributions to

this research. None of the authors has a financial conflict of interest related to this research.

REFERENCES

Auffan, M., Rose, J., Orsiere, T., de Meo, M., Thill, A., Zeyons, O., Proux, O., Masion, A., Chaurand, P., Spalla, O., *et al*. (2009). CeO2 nanoparticles induce DNA damage towards human dermal fibroblasts in vitro. *Nanotoxicology* **3,** 161–171.

Babu, S., Cho, J. H., Dowding, J. M., Heckert, E., Komanski, C., Das, S., Colon, J., Baker, C. H., Bass, M., Self, W. T., *et al*. (2010). Multicolored redox active upconverter cerium oxide nanoparticle for bio-imaging and therapeutics. *Chem. Commun. (Camb.)* **46,** 6915–6917.

Ballou, B., Lagerholm, B. C., Ernst, L. A., Bruchez, M. P., and Waggoner, A. S. (2004). Noninvasive imaging of quantum dots in mice. *Bioconjug. Chem.* **15,** 79–86.

Bouwmeester, H., Lynch, I., Marvin, H. J., Dawson, K. A., Berges, M., Braguer, D., Byrne, H. J., Casey, A., Chambers, G., Clift, M. J., *et al*. (2011). Minimal analytical characterization of engineered nanomaterials needed for hazard assessment in biological matrices. *Nanotoxicology* **5,** 1–11.

Brunner, T. J., Wick, P., Manser, P., Spohn, P., Grass, R. N., Limbach, L. K., Bruinink, A., and Stark, W. J. (2006). *In vitro* cytotoxicity of oxide nanoparticles: Comparison to asbestos, silica, and the effect of particle solubility. *Environ. Sci. Technol.* **40,** 4374–4381.

Butterfield, D. A. (1997). beta-Amyloid-associated free radical oxidative stress and neurotoxicity: Implications for Alzheimer's disease. *Chem. Res. Toxicol.* **10,** 495–506.

Cassee, F. R., van Balen, E. C., Singh, C., Green, D., Muijser, H., Weinstein, J., and Dreher, K. (2011). Exposure, health and ecological effects review of engineered nanoscale cerium and cerium oxide associated with its use as a fuel additive. *Crit. Rev. Toxicol.* **41,** 213–229.

Celardo, I., De Nicola, M., Mandoli, C., Pedersen, J. Z., Traversa, E., and Ghibelli, L. (2011). Ce^{3+} ions determine redox-dependent anti-apoptotic effect of cerium oxide nanoparticles. *ACS Nano* **5,** 4537–4549.

Chen, J., Patil, S., Seal, S., and McGinnis, J. F. (2006). Rare earth nanoparticles prevent retinal degeneration induced by intracellular peroxides. *Nat. Nanotechnol.* **1,** 142–150.

Chithrani, B. D., Ghazani, A. A., and Chan, W. C. (2006). Determining the size and shape dependence of gold nanoparticle uptake into mammalian cells. *Nano Lett.* **6,** 662–668.

Cho, W. S., Duffin, R., Poland, C. A., Howie, S. E., MacNee, W., Bradley, M., Megson, I. L., and Donaldson, K. (2010). Metal oxide nanoparticles induce unique inflammatory footprints in the lung: Important implications for nanoparticle testing. *Environ. Health Perspect.* **118,** 1699–1706.

Choi, H. S., Liu, W., Misra, P., Tanaka, E., Zimmer, J. P., Itty Ipe, B., Bawendi, M. G., and Frangioni, J. V. (2007). Renal clearance of quantum dots. *Nat. Biotechnol.* **25,** 1165–1170.

Choi, J., Reipa, V., Hitchins, V. M., Goering, P. L., and Malinauskas, R. A. (2011). Physicochemical characterization and in vitro hemolysis evaluation of silver nanoparticles. *Toxicol. Sci.* **123,** 133–143.

Choi, J. Y., Ramachandran, G., and Kandlikar, M. (2009). The impact of toxicity testing costs on nanomaterial regulation. *Environ. Sci. Technol.* **43,** 3030–3034.

Colon, J., Hsieh, N., Ferguson, A., Kupelian, P., Seal, S., Jenkins, D. W., and Baker, C. H. (2010). Cerium oxide nanoparticles protect gastrointestinal epithelium from radiation-induced damage by reduction of reactive oxygen species and upregulation of superoxide dismutase 2. *Nanomedicine* **6,** 698–705.

D'Angelo, B., Santucci, S., Benedetti, E., Di Loreto, S., Phani, R. A., Falone, S., Amicarelli, F., Ceru, M. P., and Cimini, A. (2009). Cerium oxide nanoparticles trigger neuronal survival in a human Alzheimer disease model by modulating BDNF pathway. *Curr. Nanosci.* **5,** 167–176.

Das, M., Patil, S., Bhargava, N., Kang, J. F., Riedel, L. M., Seal, S., and Hickman, J. J. (2007). Auto-catalytic ceria nanoparticles offer neuroprotection to adult rat spinal cord neurons. *Biomaterials* **28,** 1918–1925.

Durbin, P. W., Williams, M. H., Gee, M., Newman, R. H., and Hamilton, J. G. (1956). Metabolism of the lanthanons in the rat. *Proc. Soc. Exp. Biol. Med.* **91,** 78–85.

Estevez, A. Y., Pritchard, S., Harper, K., Aston, J. W., Lynch, A., Lucky, J. J., Ludington, J. S., Chatani, P., Mosenthal, W. P., Leiter, J. C., *et al*. (2011). Neuroprotective mechanisms of cerium oxide nanoparticles in a mouse hippocampal brain slice model of ischemia. *Free Radic. Biol. Med.* **51,** 1155–1163.

Fabian, E., Landsiedel, R., Ma-Hock, L., Wiench, K., Wohlleben, W., and van Ravenzwaay, B. (2008). Tissue distribution and toxicity of intravenously administered titanium dioxide nanoparticles in rats. *Arch. Toxicol.* **82,** 151–157.

Feng, X., Sayle, D. C., Wang, Z. L., Paras, M. S., Santora, B., Sutorik, A. C., Sayle, T. X., Yang, Y., Ding, Y., Wang, X., *et al*. (2006). Converting ceria polyhedral nanoparticles into single-crystal nanospheres. *Science* **312,** 1504–1508.

Gehlhaus, M., Osier, M., Llados, F., Plewak, D., Lumpkin, M., Odin, M., and Rooney, A. (2009). *Toxicological Review of Cerium Oxide and Cerium Compounds (CAS No. 1306-38-3) In support of Summary Information on the Integrated Risk Information System (IRIS).* pp. 118. U.S. Environmental Protection Agency. Available at: http://www.epa.gov/iris/toxreviews/1018tr.pdf.

He, X., Zhang, H., Ma, Y., Bai, W., Zhang, Z., Lu, K., Ding, Y., Zhao, Y., and Chai, Z. (2010). Lung deposition and extrapulmonary translocation of nanoceria after intratracheal instillation. *Nanotechnology* **21,** 285103/1–285103/8.

Health Effects Institute (HEI) (2001). *Evaluation of Human Health Risk From Cerium Added to Diesel Fuel, Communication 9*. Available at: http://pubs.healtheffects.org/getfile.php?u=295.

Hirst, S. M., Karakoti, A., Singh, S., Self, W., Tyler, R., Seal, S., and Reilly, C. M. (Forthcoming). Bio-distribution and in vivo antioxidant effects of cerium oxide nanoparticles in mice. *Environ. Toxicol.*

Hirst, S. M., Karakoti, A. S., Tyler, R. D., Sriranganathan, N., Seal, S., and Reilly, C. M. (2009). Anti-inflammatory properties of cerium oxide nanoparticles. *Small* **5,** 2848–2856.

Hussain, S. M., Hess, K. L., Gearhart, J. M., Geiss, K. T., and Schlager, J. J. (2005). In vitro toxicity of nanoparticles in BRL 3A rat liver cells. *Toxicol. In Vitro* **19,** 975–983.

Integrated Laboratory Systems (ILS). (2006). *Chemical Information Profile for Ceric Oxide [CAS No. 1306-38-3]. Supporting Nomination for Toxicological Evaluation by the National Toxicology Program.* National Toxicology Program. National Institute of Environmental Health Sciences, National Institutes of Health, U.S. Department of Health and Human Services, Research Triangle Park, NC. Available at: http://ntp.niehs.nih.gov/files/ceric_oxide2.pdf.

Jiang, J., Oberdörster, G., Elder, A., Gelein, R., Mercer, P., and Biswas, P. (2008). Does nanoparticle activity depend upon size and crystal phase? *Nanotoxicology* **2,** 33–42.

Korsvik, C., Patil, S., Seal, S., and Self, W. T. (2007). Superoxide dismutase mimetic properties exhibited by vacancy engineered ceria nanoparticles. *Chem. Commun. (Camb.)* 1056–1058.

Lin, W., Huang, Y. W., Zhou, X. D., and Ma, Y. (2006). Toxicity of cerium oxide nanoparticles in human lung cancer cells. *Int. J. Toxicol.* **25,** 451–457.

Loh, J. W., Yeoh, G., Saunders, M., and Lim, L.-Y. (2010). Uptake and cytotoxicity of chitosan nanoparticles in human liver cells. *Toxicol. Appl. Pharmacol.* **249,** 148–157.

Mai, H.-X., Sun, L.-D., Zhang, Y.-W., Si, R., Feng, W., Zhang, H.-P., Liu, H.-C., and Yan, C.-H. (2005). Shape-selective synthesis and oxygen storage behavior of ceria nanopolyhedra, nanorods, and nanocubes. *J. Phys. Chem. B* **109,** 24380–24385.

Maynard, A. D., Warheit, D. B., and Philbert, M. A. (2011). The new toxicology of sophisticated materials: Nanotoxicology and beyond. *Toxicol. Sci.* **120**(Suppl. 1), S109–S129.

Miller, J. K., and Byrne, W. F. (1970). Absorption, excretion, and tissue distribution of orally and intravenously administered radiocerium as affected by EDTA. *J. Dairy Sci.* **53,** 171–175.

Moghimi, S. M., Hunter, A. C., and Murray, J. C. (2001). Long-circulating and target-specific nanoparticles: Theory to practice. *Pharmacol. Rev.* **53,** 283–318.

Molin, S., Gazda, M., Jasinski, P., and Nowakowski, A. (2008). Electrical properties of porous nanocrystalline undoped ceria oxygen sensor. *Elektronika* **49,** 253–254.

Nel, A., Xia, T., Madler, L., and Li, N. (2006). Toxic potential of materials at the nanolevel. *Science* **311,** 622–627.

Nel, A. E., Madler, L., Velegol, D., Xia, T., Hoek, E. M., Somasundaran, P., Klaessig, F., Castranova, V., and Thompson, M. (2009). Understanding biophysicochemical interactions at the nano-bio interface. *Nat. Mater.* **8,** 543–557.

Niu, J., Azfer, A., Rogers, L. M., Wang, X., and Kolattukudy, P. E. (2007). Cardioprotective effects of cerium oxide nanoparticles in a transgenic murine model of cardiomyopathy. *Cardiovasc. Res.* **73,** 549–559.

Niu, J., Wang, K., and Kolattukudy, P. E. (2011). Cerium oxide nanoparticles inhibit oxidative stress and nuclear factor-kappaB activation in H9c2 cardiomyocytes exposed to cigarette smoke extract. *J. Pharmacol. Exp. Ther.* **338,** 53–61.

Organisation for Economic Co-operation and Development (OECD) (2010). *List of Manufactured Nanomaterials and List of Endpoints for Phase One of the Sponsorship Programme for the Testing of Manufactured Nanomaterials: Revision*. Environment Directorate, Pesticides and Biotechnology, Organisation for Economic Co-operation and Development. Paris. pp. 16, ENV/JM/MONO(2010)46, http://www.oecd.org/officialdocuments/displaydocumentpdf?cote=env/jm/mono(2010)46&doclanguage=en.

Okon, E. E., Pulikan, D., Pereverzev, A. E., Kudriavtsev, B. N., and Zhale, P. (2000). Toxicity of magnetite-dextran particles: Morphological study. *Tsitologiia* **42,** 358–366.

Park, B., Martin, P., Harris, C., Guest, R., Whittingham, A., Jenkinson, P., and Handley, J. (2007). Initial in vitro screening approach to investigate the potential health and environmental hazards of Envirox™—A nanoparticulate cerium oxide diesel fuel additive. *Part. Fibre Toxicol.* **4,** 12.

Park, E. J., Choi, J., Park, Y. K., and Park, K. (2008). Oxidative stress induced by cerium oxide nanoparticles in cultured BEAS-2B cells. *Toxicology* **245,** 90–100.

Park, E.-J., Park, Y.-K., and Park, K. (2009). Acute toxicity and tissue distribution of cerium oxide nanoparticles by a single oral administration in rats. *Toxicol. Res.* **25,** 79–84.

Park, E.-J., Wan-Seob, C., Jeong, J., Yi, J.-H., Choi, K., Kim, Y., and Park, K. (2010). Induction of inflammatory responses in mice treated with cerium oxide nanoparticles by intratracheal instillation. *J. Health Sci.* **56,** 387–396.

Patlolla, A., Berry, A., and Tchounwou, P. (2011). Study of hepatotoxicity and oxidative stress in male Swiss-Webster mice exposed to functionalized multi-walled carbon nanotubes. *Mol. Cell. Biochem.* **358,** 189–199.

Pirmohamed, T., Dowding, J. M., Singh, S., Wasserman, B., Heckert, E., Karakoti, A. S., King, J. E., Seal, S., and Self, W. T. (2010). Nanoceria exhibit redox state-dependent catalase mimetic activity. *Chem. Commun. (Camb.)* **46,** 2736–2738.

Powers, K. W., Palazuelos, M., Brown, S. C., and Roberts, S. M. (2009). Characterization of nanomaterials for toxicological evaluation. In *Nanotoxicology From* In Vivo *and* In Vitro *Models to Health Risks*. (S. Sahu and D. Casciano, Eds.), pp. 1–27. Wiley, Chichester, West Sussex, U.K.

Rodea-Palomares, I., Boltes, K., Fernandez-Pinas, F., Leganes, F., Garcia-Calvo, E., Santiago, J., and Rosal, R. (2011). Physicochemical characterization and ecotoxicological assessment of CeO2 nanoparticles using two aquatic microorganisms. *Toxicol. Sci.* **119,** 135–145.

Roh, J. Y., Park, Y. K., Park, K., and Choi, J. (2010). Ecotoxicological investigation of CeO(2) and TiO(2) nanoparticles on the soil nematode Caenorhabditis elegans using gene expression, growth, fertility, and survival as endpoints. *Environ. Toxicol. Pharmacol.* **29,** 167–172.

Sayes, C. M., Gobin, A. M., Ausman, K. D., Mendez, J., West, J. L., and Colvin, V. L. (2005). Nano-C60 cytotoxicity is due to lipid peroxidation. *Biomaterials* **26,** 7587–7595.

Sayes, C. M., and Warheit, D. B. (2009). Characterization of nanomaterials for toxicity assessment. *Wiley Interdiscip. Rev. Nanomed. Nanobiotechnol.* **1,** 660–670.

Srinivas, A., Rao, P. J., Selvam, G., Murthy, P. B., and Reddy, P. N. (2011). Acute inhalation toxicity of cerium oxide nanoparticles in rats. *Toxicol. Lett.* **205,** 105–115.

Stadtman, E. R. (2006). Protein oxidation and aging. *Free Radic. Res.* **40,** 1250–1258.

Sultana, R., Ravagna, A., Mohmmad-Abdul, H., Calabrese, V., and Butterfield, D. A. (2005). Ferulic acid ethyl ester protects neurons against amyloid beta-peptide(1-42)-induced oxidative stress and neurotoxicity: Relationship to antioxidant activity. *J. Neurochem.* **92,** 749–758.

Sung, J. H., Ji, J. H., Park, J. D., Yoon, J. U., Kim, D. S., Jeon, K. S., Song, M. Y., Jeong, J., Han, B. S., Han, J. H., *et al.* (2009). Subchronic inhalation toxicity of silver nanoparticles. *Toxicol. Sci.* **108,** 452–461.

Thill, A., Zeyons, O., Spalla, O., Chauvat, F., Rose, J., Auffan, M., and Flank, A. M. (2006). Cytotoxicity of CeO_2 nanoparticles for *Escherichia coli*. Physico-chemical insight of the cytotoxicity mechanism. *Environ. Sci. Technol.* **40,** 6151–6156.

Tseng, M. T., Lu, X., Duan, X., Hardas, S. S., Sultana, R., Wu, P., Unrine, J. M., Graham, U., Butterfield, D. A., Grulke, E., *et al.* (2012). Hepatic structural and oxidative stress indices alteration by intravenous infusion of nanoceria. *Toxicol. Appl. Pharmacol.* **260,** 173–182.

Van Hoecke, K., Quik, J. T. K., Mankiewicz-Boczek, J., De Schamphelaere, K. A. C., Elsaesser, A., Van der Meeren, P., Barnes, C., McKerr, G., Vyvyan Howard, C., Van De Meent, D., *et al.* (2009). Fate and effects of CeO_2 nanoparticles in aquatic ecotoxicity tests. *Environ. Sci. Technol.* **43,** 4537–4546.

Wang, J., Chen, B., Jin, N., Xia, G., Chen, Y., Zhou, Y., Cai, X., Ding, J., Li, X., and Wang, X. (2011). The changes of T lymphocytes and cytokines in ICR mice fed with Fe3O4 magnetic nanoparticles. *Int. J. Nanomedicine* **6,** 605–610.

Wang, J., Chen, C., Lau, S., Raghavan, R. I., Rowsell, E. H., Said, J., Weiss, L. M., and Huang, Q. (2009). CD3-positive large B-cell lymphoma. *Am. J. Surg. Pathol.* **33,** 505–512.

Warheit, D. B., Sayes, C. M., Reed, K. L., and Swain, K. A. (2008). Health effects related to nanoparticle exposures: Environmental, health and safety considerations for assessing hazards and risks. *Pharmacol. Ther.* **120,** 35–42.

Xia, T., Kovochich, M., Liong, M., Madler, L., Gilbert, B., Shi, H., Yeh, J. I., Zink, J. I., and Nel, A. E. (2008). Comparison of the mechanism of toxicity of zinc oxide and cerium oxide nanoparticles based on dissolution and oxidative stress properties. *ACS Nano* **2,** 2121–2134.

Yokel, R. A., Florence, R. L., Unrine, J. M., Tseng, M. T., Graham, U. M., Wu, P., Grulke, E. A., Sultana, R., Hardas, S. S., and Butterfield, D. A. (2009). Biodistribution and oxidative stress effects of a systemically-introduced commercial ceria engineered nanomaterial. *Nanotoxicology* **3,** 234–248.

Younce, C. W., Wang, K., and Kolattukudy, P. E. (2010). Hyperglycaemia-induced cardiomyocyte death is mediated via MCP-1 production and induction of a novel zinc-finger protein MCPIP. *Cardiovasc. Res.* **87,** 665–674.

Yuan, J., Gao, H., Sui, J., Chen, W. N., and Ching, C. B. (2011). Cytotoxicity of single-walled carbon nanotubes on human hepatoma HepG2 cells: An iTRAQ-coupled 2D LC–MS/MS proteome analysis. *Toxicol. In Vitro* **25,** 1820–1827.

Yuan, Q., Duan, H.-H., Li, L.-L., Sun, L.-D., Zhang, Y.-W., and Yan, C.-H. (2009). Controlled synthesis and assembly of ceria-based nanomaterials. *J. Colloid Interface Sci.* **335,** 151–167.

Zeyons, O., Thill, A., Chauvat, F., Menguy, N., Cassier-Chauvat, C., Orear, C., Daraspe, J., Auffan, M., Rose, J., and Spalla, O. (2009). Direct and indirect CeO2 nanoparticles toxicity for Escherichia coli and Synechocystis. *Nanotoxicology* **3,** 284–295.

Zhang, H., He, X., Zhang, Z., Zhang, P., Li, Y., Ma, Y., Kuang, Y., Zhao, Y., and Chai, Z. (2010). Nano-CeO2 exhibits adverse effects at environmental relevant concentrations. *Environ. Sci. Technol.* **45,** 3725–3730.

Zhou, X., Wong, L. L., Karakoti, A. S., Seal, S., and McGinnis, J. F. (2011). Nanoceria inhibit the development and promote the regression of pathologic retinal neovascularization in the Vldlr knockout mouse. *PLoS One* **6,** e16733.